

# Ab-initio study of ultrafast charge dynamics in graphene

Q. Z. Li<sup>1</sup>, P. Elliott<sup>1</sup>, J. K. Dewhurst<sup>2</sup>, S. Sharma<sup>1</sup> and S. Shallcross<sup>1</sup>

*1 Max-Born-Institute for Non-linear Optics and and Short Pulse Spectroscopy,  
Max-Born Strasse 2A, 12489 Berlin, Germany and*

*2 Max-Planck-Institut für Mikrostrukturphysik Weinberg 2, D-06120 Halle, Germany.*

Monolayer graphene provides an ideal material to explore one of the fundamental light-field driven interference effects: Landau-Zener-Stückelberg interference. However, direct observation of the resulting interference patterns in momentum space has not proven possible, with Landau-Zener-Stückelberg interference observed only indirectly through optically induced residual currents. Here we show that the transient electron momentum density (EMD), an object that can easily be obtained in experiment, provides an excellent description of momentum resolved charge excitation. We employ state-of-the-art time-dependent density function theory calculations, demonstrating by direct comparison of EMD with conduction band occupancy, obtained from projecting the time propagated wavefunction onto the ground state, that the two quantities are in excellent agreement. For even the most intense laser pulses we find that the electron dynamics to be almost completely dominated by the  $\pi$ -band, with transitions to other bands strongly suppressed. Simple model based tight-binding approaches can thus be expected to provide an excellent description for the laser induced electron dynamics in graphene.

Intense laser light offers the possibility to control electrons in matter on femtosecond time scales. Triumphs of this burgeoning field include tuning the optically induced current in graphene via the carrier envelope phase of light<sup>1-3</sup>, attosecond control over magnetic order in thin films of magnetic overlayers<sup>4,5</sup>, and controlled valley excitation in the semi-conducting few layer dichalcogenides by circularly polarized light<sup>6,7</sup> to name only a few examples. The two band Dirac cone found in graphene provides an ideal in materials platform for studying one of the canonical light-field driven interference effects: Landau-Zener-Stückelberg (LZS) interference<sup>8,9</sup>, which before its observation in graphene<sup>3</sup> had only been observed in designed two state quantum systems<sup>10-14</sup>. This effect occurs when an oscillating electromagnetic field drives intraband oscillation through the Bloch acceleration theorem  $\mathbf{k} \rightarrow \mathbf{k} + \mathbf{A}(t)$  and in the region of an avoided crossing interband transitions occur even when the band gap exceeds the dominant pulse frequency, so-called Landau-Zener transitions. Upon repeated passing of the avoided crossing multiple pathways exist to the conduction band with consequent constructive and destructive interference of electron states. This offers rich possibilities for controlling electron dynamics by intense laser light, demonstrated by the recent observation of control over optical currents underpinned by LZS interference<sup>3</sup>, a result anticipated theoretically in Ref. 15.

The ubiquity of the avoided crossing band structure in 2d materials, found not only in the Dirac cone of graphene but also in the the semi-conducting monolayer dichalcogenides<sup>16</sup>, phosphorene<sup>17</sup>, silicene<sup>18</sup>, and stanene<sup>19</sup>, points towards the importance of LSZ interferometry in controlling electron dynamics in 2d materials. However, while interference physics can be easily probed theoretically through the conduction band population<sup>20,21</sup>, the experimental situation is more difficult, with to date only indirect observations of LSZ physics in materials reported. In this paper we show

that the transient electron momentum density (EMD) difference, defined as

$$\Delta\rho(\mathbf{p}, t_f) = \rho(\mathbf{p}, t_f) - \rho(\mathbf{p}, t = 0) \quad (1)$$

with  $\mathbf{p}$  momentum and  $\rho(\mathbf{p}, t)$  the electron momentum density<sup>22</sup> before ( $t = 0$ ) and after ( $t_f$ ) the pump laser pulse, offers a tool for directly probing LZS interference effects. As transient EMD is a practical probe experimentally<sup>23,24</sup>, this suggests a way in which the LZS physics may be directly observed in 2d materials, opening the way to correlate indirect LZS physics such as induced currents with the fundamental momentum space interference patterns.

In contrast to previous works that have employed simple single particle tight-binding Hamiltonians to study the LZS effect<sup>3,20,21,25-29</sup>, we will here deploy the time dependent version of density functional theory (TD-DFT). To establish the accuracy of the EMD as a record of LZS interference we compare it with the excited electron distribution,  $N_{\text{ex}}$ , defined within TD-DFT as<sup>30</sup>:

$$N_{\text{ex}}(\mathbf{k}, t) = \sum_i^{\text{occ}} \sum_j^{\text{unocc}} |\langle \psi_{i\mathbf{k}}(t) | \psi_{j\mathbf{k}}(t = 0) \rangle|^2 \quad (2)$$

where  $\psi_{j\mathbf{k}}(t)$  is the time-dependent Kohn-Sham orbital at time  $t$ , and  $\psi_{i\mathbf{k}}(t = 0)$  is the ground state orbital. In all cases we find that the pattern of excitation in momentum space generated by transient EMD and  $N_{\text{ex}}$  is nearly identical in the first BZ.

Finally, we consider the role of the non- $\pi$ -band states in the electron dynamics in graphene. Remarkably, despite electron excitation through the whole energy range of the  $\pi$ -band (up to 10 eV above the Fermi energy, an energy range encompassing the  $\sigma^*$  bands as well as several high  $l$  character bands), it turns out that there occur almost no transitions to states outside the  $\pi$ -band

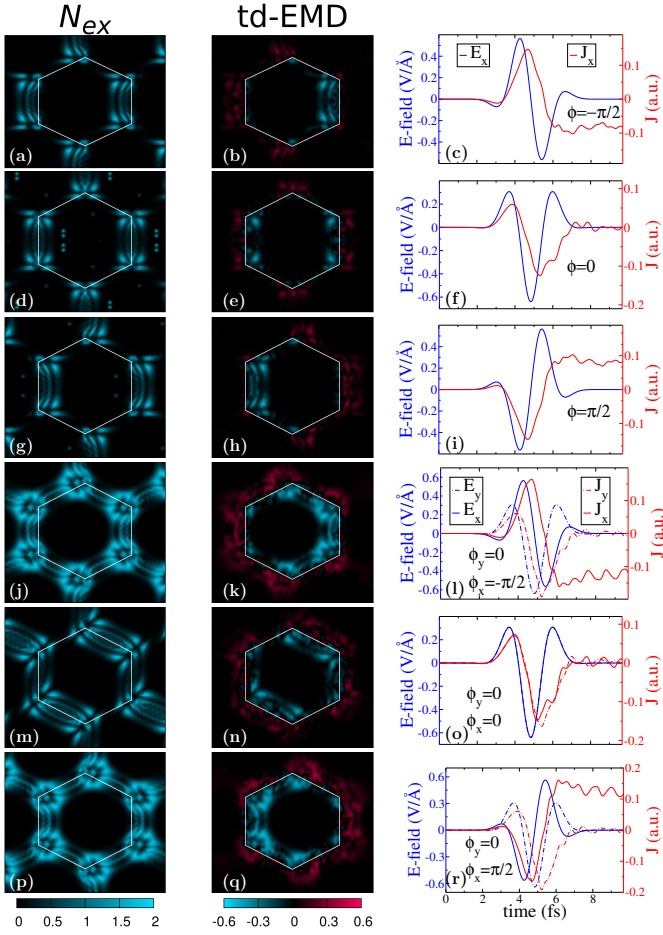


Figure 1: Conduction band occupation as a function of  $\mathbf{k}$ -vector as determined directly by projection of the time-dependent state onto the ground-state Kohn-Sham states (first column), see Eq. (2), and, second column, the transient electron momentum density (td-EMD) difference, see Eq. (1). Evidently, both quantities in a consistent way capture the momentum space intensity fringes generated by Landau-Zener-Stückelberg interference in the first BZ. This depends sensitively on the momentum space path induced by the laser pulse as evidenced by the dependence on carrier envelope phase  $\phi$  (CEP) and polarization. The CEP values are given in the third column which displays the electric field of the pump laser pulse and induced current density. All pulses have the same full width half maximum (FWHM) of 1.935 fs, a central frequency of 1.4 eV, and peak intensity of  $5.43 \times 10^{12}$  W/cm<sup>2</sup>. In the first and second columns, the white hexagons represent the boundary of the 1st BZ.

manifold. We attribute this to the near vanishing of the corresponding dipole matrix elements. Our calculations thus suggest that even for very significant laser excitation tight-binding based models will provide a good description of the electron dynamics.

According to Runge-Gross theorem<sup>31</sup>, which extends the Hohenberg-Kohn theorem into the time domain, with common initial states there will be a one to one correspondence between the time-dependent external poten-

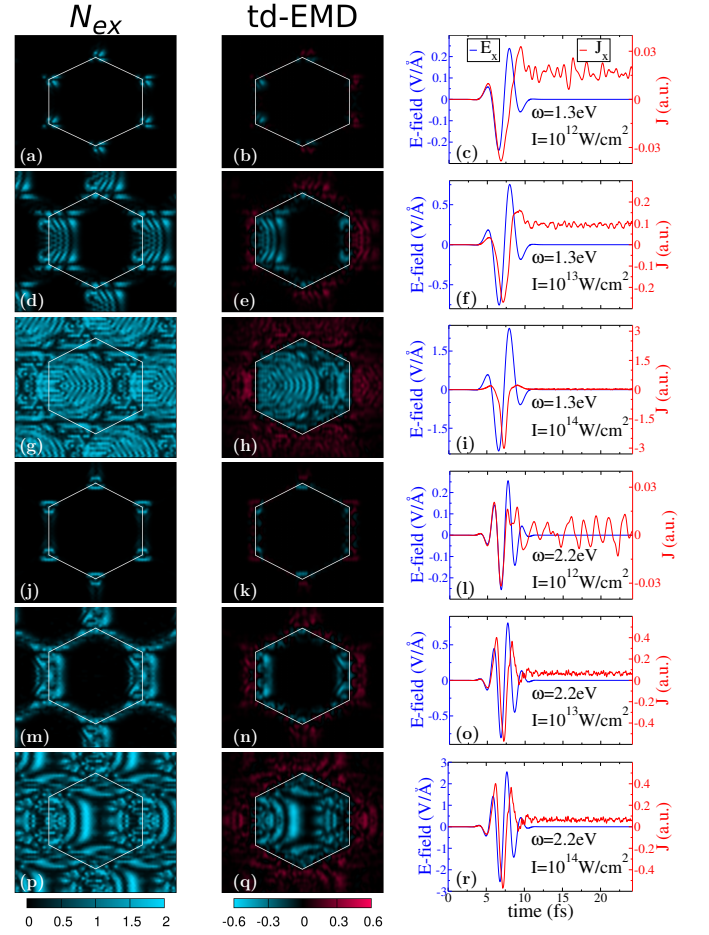


Figure 2: Dependence of Landau-Zener-Stückelberg interference fringes on pulse intensity and frequency. Each row represents a different pulse with the frequency and intensity shown in the inset of the third column panels (in all cases the full width half maximum (FWHMs) was 2.758 fs, and carrier envelope phase (CEP) was  $\frac{\pi}{2}$ ). Shown in the first column is the conduction band occupation as a function of  $\mathbf{k}$ -vector determined by directly projecting the time propagated wavefunction onto the ground-state Kohn-Sham orbitals (first column), see Eq. (2). The second column displays the transient electron momentum density (td-EMD) difference, see Eq. (1) for definition. Evidently, both quantities capture in a consistent way the momentum space intensity fringes resulting from Landau-Zener-Stückelberg interference. The third column shows the residual current density induced by the pulse, along with the pump pulse electric field,  $\mathbf{E}(t)$ . In the first and second columns, the white hexagons indicate the boundaries of the 1st BZ.

tials and densities<sup>32,33</sup>. Based on this theorem, a system of non-interacting particles can be chosen such that the density of this non-interacting system is equal to that of the interacting system for all times, with the wave function of this non-interacting system represented by a Slater determinant of single-particle orbitals. These time-dependent Kohn-Sham (KS) orbitals are governed by the Schrödinger equation (for the spin degenerate case):

$$i\partial_t\psi_j(\mathbf{r},t) = \left[ \frac{1}{2} \left( -i\nabla + \frac{1}{c} \mathbf{A}_{\text{ext}}(t) \right)^2 + v_s(\mathbf{r},t) \right] \psi_j(\mathbf{r},t). \quad (3)$$

In the above equation  $\mathbf{A}_{\text{ext}}(t)$  is the vector potential representing the applied laser field, the effective potential  $v_s(\mathbf{r},t)$  is given by  $v_s(\mathbf{r},t) = v_{\text{ext}}(\mathbf{r},t) + v_{\text{H}}(\mathbf{r},t) + v_{\text{xc}}(\mathbf{r},t)$ , where  $v_{\text{ext}}(\mathbf{r},t)$  is the external potential,  $v_{\text{H}}(\mathbf{r},t)$  the Hartree potential, and  $v_{\text{xc}}(\mathbf{r},t)$  is the exchange-correlation (xc) potential. For the latter we have used the adiabatic local density approximation. From the Fourier transform of the Kohn-Sham states,  $\psi_{i\mathbf{k}}(\mathbf{r})$ , the electron momentum density can be constructed as  $\rho(\mathbf{p}) = \sum_{i\mathbf{k}} |\psi_{i\mathbf{k}}(\mathbf{p})|^2$ . This EMD constructed from KS states has been found to provide excellent agreement with that obtained from Compton scattering<sup>22</sup>.

All the calculations are performed by employing the state-of-the-art all-electron full potential linearized augmented plane wave (LAPW) method<sup>34</sup>, as implemented in the ELK code<sup>35</sup>. We have used  $30 \times 30$   $\mathbf{k}$ -point set; for further details of the implementation of TD-DFT within the LAPW basis we refer the reader to Refs. 36 and 37.

*LZS interference probed by 2D td-EMD:* the patterns of excited charge in momentum space that most directly characterise Landau-Zener-Stückelberg interference are generally presented by plotting the conduction band occupation over the first Brillouin zone. However this information, while easy to obtain theoretically, is difficult to obtain experimentally. We thus look at an alternative quantity, the change in electron momentum density due to the laser pulse.

In Fig. 1 we consider a few cycle pulse of full width half maximum 1.935 fs, central frequency 1.4 eV and a peak pulse intensity of  $5.43 \times 10^{12}$  W/cm<sup>2</sup>. We vary the pulse carrier envelope phase (the angular difference between the  $\mathbf{E}$ -field and pulse envelope maxima) for various pulse polarizations,  $y$ -polarized (shown in Fig. 1 (a-i)), circularly polarized (Fig. 1 (j-l) and (p-q)), and linearly polarized (Fig. 1(m-o)). The magnitude of the electric field is of the order of 5 V/nm, which places these pulses in the strong non-perturbative regime for graphene. The  $\mathbf{A}$ -field can drive several passes of the gap that occurs on any constant momentum slice that does not pass through the Dirac point. These repeated crossings of the gap minima generate multiple electron pathways from valence to conduction band and concomitant interference effects. In the first and second columns of Fig. 1 are shown the number of excited electrons  $N_{\text{ex}}$  (Eq. (2)) and the EMD (Eq. (1)) respectively. Evidently, these two objects convey consistent information concerning the excited charge distribution.

A striking asymmetry of charge excitation in the 1BZ as a function of the carrier envelope phase (CEP) can be observed, compare panels (a), (d), and (g) of Fig. 1. Carrier envelope phases (CEP) of  $\phi = +\pi/2$  and  $-\pi/2$

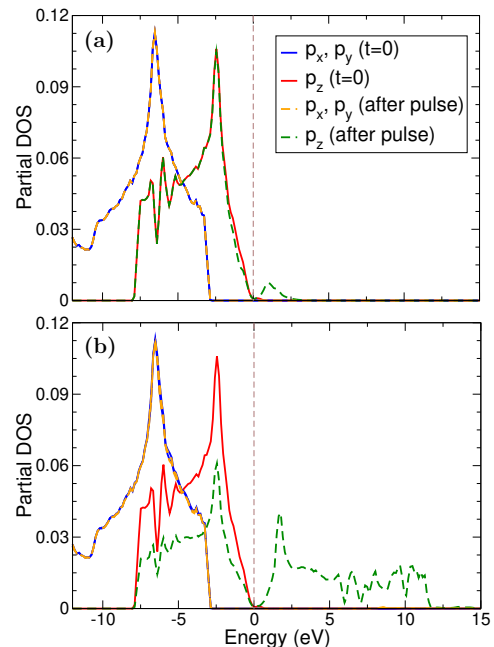


Figure 3: Time dependent partial density of states (PDOS) projected onto the  $l = 1$  spherical harmonics. Here the PDOS (in states/atom/eV) is shown both at  $t = 0$  before the pulse, and at the end of the simulation after the pulse has been applied. The pump pulse for panels (a) and (b) is polarized in the  $x$ -direction, with intensities  $10^{12}$  W/cm<sup>2</sup> and  $10^{14}$  W/cm<sup>2</sup> respectively. As can be seen, even for almost complete excitation of the  $\pi$ -band in which charge is excited from the  $\pi$ -band minima up to the  $\pi^*$ -band maxima, there is no excitation into states of  $p_x$  or  $p_y$  character.

displays pronounced excitation for  $k_x < 0$  and  $k_x > 0$  respectively, while for  $\phi = 0$  the excitation is symmetric in  $k_x$  (we here measure momentum from the high symmetry K point). This asymmetry is a consequence of the fact that for non-zero CEP the  $\mathbf{A}(t)$  field executes motion in momentum space breaking the  $k_x$  mirror symmetry<sup>3</sup>. Interestingly, it can also be seen that the momentum space excitations weakly break symmetry in  $k_y$  as well.

In Fig. 2 are displayed the  $N_{\text{ex}}$  and EMD for a pulses of central frequency 1.3 eV and intensities  $10^{12}$  W/cm<sup>2</sup>,  $10^{13}$  W/cm<sup>2</sup>,  $10^{14}$  W/cm<sup>2</sup> (Fig. 2 (a-i)) and a frequency 2.2 eV with the same intensities (Fig. 2 (j-r)). Once again the very good agreement between the  $N_{\text{ex}}$  and EMD can be noted. Increasing the intensity results in the LZS interference fringes (the lines of high probability density in momentum space) extending increasingly far from the BZ boundary, a fact that follows from the increase in the vector potential maximum which, by the Bloch acceleration theorem, results in electron trajectories extending further into momentum space. Taken together, these results demonstrate that EMD generates a map of momentum space excitations carrying nearly identical information to the conduction band occupancy in the 1st BZ, and thus represents an ideal experimental tool for studying the fundamental interference patterns of the LZS effect.

*The residual current:* In the past asymmetric LZS interference has been indirectly accessed by means the net

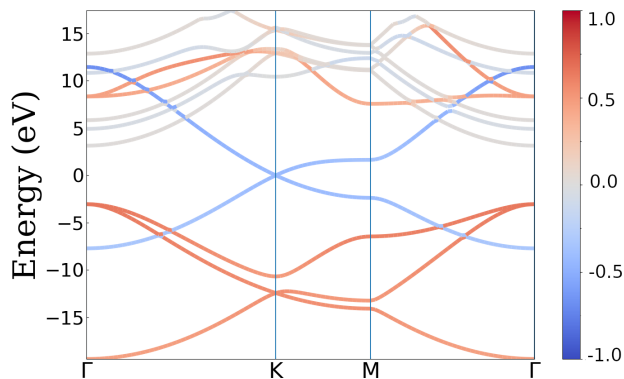


Figure 4: Band structure of graphene showing the  $\pi$  and  $\sigma$  band character. Negative and positive numbers indicate dominance by  $\pi$ - and  $\sigma$ -character respectively.

current induced by the laser pulse<sup>3</sup>. For non-zero carrier envelope phase, i.e. a lightwave in which the  $\mathbf{E}$ -field maximum is displaced from the pulse envelope maximum, the asymmetric momentum space trajectories generate excitations that result in a net current. To date this represents the only observation in experiment of LSZ in a material<sup>3</sup>. Underpinning this residual current is an early time coherent steady current, that ultimately at longer time scales generates heating, and the diffusive residual current measured in experiment. This coherent current (current per unit cell) induced by the laser pulse is displayed in the third column of Figs. 1 and 2. All pump pulses with a non-zero CEP can be seen to induce such a steady state current, with the change of sign of the current with CEP reflecting the asymmetric momentum space excitations seen in the first two columns of Figs. 1 and 2. As the momentum space trajectories travel further from the Dirac point (e.g. by increasing the intensity of the pulse), the current initially increases, correlating with an increased asymmetry in the excited charge (see Fig. 2 d-f), before widespread excitation throughout the BZ results in overall cancellation of current carrying states and a very small residual current for the most intense 1 eV pulse (see Fig. 2 g-i). A similar picture can be seen for the 2 eV pulse, however here the decreased asymmetry in the excited charge results in a reduced current. We thus see that the magnitude of the induced current correlates well with the asymmetry of excited charge in momentum space, although as stressed by Motlagh *et al.*<sup>38</sup> the optically induced current is in general not governed solely by the momentum space distribution of excited charge.

*Dominance of the  $\pi$ -manifold in electron dynamics:* the results for the momentum resolved conduction band occupation shown in the previous sections, correspond very closely to results obtained on the basis of model  $\pi$ -band only tight-binding Hamiltonians. This raises the question of whether this is due simply to the relatively low energies of the excited charge (in Fig 1 and Fig. 2 the excited charge resides predominantly at the K point and the K-M-K line) or whether, for a more general reason, the  $\pi$ -band will always dominate ultrafast laser induced

electron dynamics in graphene.

To explore this in Fig. 3 we display the partial density of states calculated before and after the laser pulse. As can be seen, see Fig. 3a, for the pulse of intensity  $10^{12}$  W/cm<sup>2</sup>, the partial DOS after the pulse shows conduction band occupation only up to 2.5 eV. At these energies, see Fig. 4, only the  $\pi$ -band is available for excited charge. Remarkably, when we consider a very strong pulse of intensity  $10^{14}$  W/cm<sup>2</sup> the excited electrons are again only of  $p_z$  character, Fig. 3b, despite the fact that the laser pulse is sufficiently strong to excite charge from the minima of the  $\pi$ -manifold up to the maxima of the  $\pi^*$ -manifold. As may be noted from the band structure, Fig. 4, within this energy range exist many other bands that would, in principle, be expected to be involved in the electron dynamics at such high energies.

Examination of the relevant dipole matrix elements reveals that transitions from  $\pi$  to  $\sigma^*$  and  $\pi^*$  to  $\sigma$  are negligible for laser pulses with in-plane polarization. Thus even in the highly non-perturbative regime transitions from the ground state to the  $\sigma^*$  manifold will be strongly suppressed. It might be argued that the partial DOS, a projection within (touching) muffin tins, does not account for excitation to delocalized bands of high  $l$  character. Comparison of the interstitial density of states before and after the pulse shows that there is indeed an increase in interstitial charge at around 9 eV, possibly indicating transitions from the  $\pi^*$  manifold to delocalized bands (note the intersections between  $\pi^*$  and high  $l$  character bands on the M- $\Gamma$  line), however this is a rather small effect. It would thus appear that the model  $\pi$ -band only tight-binding Hamiltonians provide an excellent description of the electron dynamics even for very intense laser pulses.

To summarize we have investigated *ab-initio* the laser induced electron dynamics in monolayer graphene. This system provides a canonical example of a material for which Landau-Zener-Stückelberg interferometry can be explored, and we have shown that direct visualisation of the interference fringes in momentum space is possible via the transient electron momentum density (EMD), establishing transient EMD as an excellent experimental tool for exploring LZS interference in 2d materials.

Examination of the excited state partial density of states reveals that the  $\pi$ -band manifold decisively dominates ultrafast laser induced dynamics in graphene, justifying the deployment of the popular Hückel tight-binding model. Whether this remains true for the complex few layer graphene systems, for which such an approach is the only one that can reasonably be envisioned, remains an open question.

## I. ACKNOWLEDGEMENTS

QZL would like to thank DFG for funding through TRR227 (project A04). SS would like to thank DFG for funding through SH498/4-1 and PE acknowledges fund-



ing from DFG Eigene Stelle project 2059421. The authors acknowledge the North-German Supercomputing

Alliance (HLRN) for providing HPC resources that have contributed to the research results reported in this paper.

- <sup>1</sup> Agustin Schiffrin, Tim Paasch-Colberg, Nicholas Karpowicz, Vadym Apalkov, Daniel Gerster, Sascha Mühlbrandt, Michael Korbman, Joachim Reichert, Martin Schultze, Simon Holzner, Johannes V. Barth, Reinhard Kienberger, Ralph Ernstorfer, Vladislav S. Yakovlev, Mark I. Stockman, and Ferenc Krausz. Optical-field-induced current in dielectrics. *Nature*, 493:70–74, 1 2013.
- <sup>2</sup> Christian Heide, Takuya Higuchi, Heiko B. Weber, and Peter Hommelhoff. Coherent electron trajectory control in graphene. *Physical Review Letters*, 121:207401, 2018.
- <sup>3</sup> Takuya Higuchi, Christian Heide, Konrad Ullmann, Heiko B. Weber, and Peter Hommelhoff. Light-field-driven currents in graphene. *Nature*, 550:224–228, 2017.
- <sup>4</sup> John Kay Dewhurst, Peter Elliott, Sam Shallcross, Eberhard K. U. Gross, and Sangeeta Sharma. Laser-Induced Intersite Spin Transfer. *Nano Letters*, 18(3):1842–1848, March 2018.
- <sup>5</sup> Florian Siegrist, Julia A. Gessner, Marcus Ossiander, Christian Denker, Yi Ping Chang, Malte C. Schröder, Alexander Guggenmos, Yang Cui, Jakob Walowski, Ulrike Martens, J. K. Dewhurst, Ulf Kleineberg, Markus Münzenberg, Sangeeta Sharma, and Martin Schultze. Light-wave dynamic control of magnetism. *Nature*, 571:240–244, 7 2019.
- <sup>6</sup> Kin Fai Mak, Keliang He, Jie Shan, and Tony F. Heinz. Control of valley polarization in monolayer MoS<sub>2</sub> by optical helicity. *Nature Nanotechnology*, 7(8):494–498, August 2012. Number: 8 Publisher: Nature Publishing Group.
- <sup>7</sup> Hualing Zeng, Junfeng Dai, Wang Yao, Di Xiao, and Xiaodong Cui. Valley polarization in MoS<sub>2</sub> monolayers by optical pumping. *Nature Nanotechnology*, 7(8):490–493, August 2012. Number: 8 Publisher: Nature Publishing Group.
- <sup>8</sup> S.N. Shevchenko, S. Ashhab, and Franco Nori. Landau–zener–stückelberg interferometry. *Physics Reports*, 492:1–30, 7 2010.
- <sup>9</sup> Ya. I. Rodionov, K. I. Kugel, and Franco Nori. Floquet spectrum and driven conductance in dirac materials: Effects of landau-zener-stückelberg-majorana interferometry. *Phys. Rev. B*, 94:195108, Nov 2016.
- <sup>10</sup> Hugo Ribeiro, J. R. Petta, and Guido Burkard. Interplay of charge and spin coherence in landau-zener-stückelberg-majorana interferometry. *Phys. Rev. B*, 87:235318, Jun 2013.
- <sup>11</sup> J. Stehlik, Y. Dovzhenko, J. R. Petta, J. R. Johansson, F. Nori, H. Lu, and A. C. Gossard. Landau-zener-stückelberg interferometry of a single electron charge qubit. *Phys. Rev. B*, 86:121303, Sep 2012.
- <sup>12</sup> F. Forster, G. Petersen, S. Manus, P. Hänggi, D. Schuh, W. Wegscheider, S. Kohler, and S. Ludwig. Characterization of qubit dephasing by landau-zener-stückelberg-majorana interferometry. *Phys. Rev. Lett.*, 112:116803, Mar 2014.
- <sup>13</sup> E. Dupont-Ferrier, B. Roche, B. Voisin, X. Jehl, R. Wacquez, M. Vinet, M. Sanquer, and S. De Franceschi. Coherent coupling of two dopants in a silicon nanowire probed by landau-zener-stückelberg interferometry. *Phys. Rev. Lett.*, 110:136802, Mar 2013.
- <sup>14</sup> X. Mi, S. Kohler, and J. R. Petta. Landau-zener interferometry of valley-orbit states in si/sige double quantum dots. *Phys. Rev. B*, 98:161404, Oct 2018.
- <sup>15</sup> Kenichi L. Ishikawa. Electronic response of graphene to an ultrashort intense terahertz radiation pulse. *New Journal of Physics*, 15(5):055021, May 2013. Publisher: IOP Publishing.
- <sup>16</sup> A. C. Dias, Fanyao Qu, David L. Azevedo, and Jiyong Fu. Band structure of monolayer transition-metal dichalcogenides and topological properties of their nanoribbons: Next-nearest-neighbor hopping. *Phys. Rev. B*, 98:075202, Aug 2018.
- <sup>17</sup> Kiho Cho, Jiong Yang, and Yuerui Lu. Phosphorene: An emerging 2d material. *Journal of Materials Research*, 32(15):2839–2847, 2017.
- <sup>18</sup> Joelson C. Garcia, Denille B. de Lima, Lucy V. C. Assali, and João F. Justo. Group iv graphene- and graphane-like nanosheets. *The Journal of Physical Chemistry C*, 115(27):13242–13246, 2011.
- <sup>19</sup> Yong Xu, Binghai Yan, Hai-Jun Zhang, Jing Wang, Gang Xu, Peizhe Tang, Wenhui Duan, and Shou-Cheng Zhang. Large-gap quantum spin hall insulators in tin films. *Phys. Rev. Lett.*, 111:136804, Sep 2013.
- <sup>20</sup> Fatemeh Nematollahi, Vadym Apalkov, and Mark I. Stockman. Phosphorene in ultrafast laser field. *Physical Review B*, 97:1–6, 2018.
- <sup>21</sup> Hamed Koochaki Kellardeh, Vadym Apalkov, and Mark I. Stockman. Attosecond strong-field interferometry in graphene: Chirality, singularity, and berry phase. *Physical Review B*, 93:1–7, 2016.
- <sup>22</sup> D Ernsting, D Billington, T D Haynes, T E Millichamp, J W Taylor, J A Duffy, S R Giblin, J K Dewhurst, and S B Dugdale. Calculating electron momentum densities and compton profiles using the linear tetrahedron method. *Journal of Physics: Condensed Matter*, 26(49):495501, nov 2014.
- <sup>23</sup> M. Samsel-Czekala, G. Kontrym-Sznajd, G. Doring, W. Schülke, J. Kwiatkowska, F. Maniawski, S. Kaprzyk, and A. Bansil. Electron momentum density in cu<sub>0.9</sub>al<sub>0.1</sub>. *Applied Physics A: Materials Science and Processing*, 76:87–92, 2003.
- <sup>24</sup> F. F. Kurp, Th Tschentscher, H. Schulte-Schrepping, J. R. Schneider, and F. Bell. 3d-electron momentum density of graphite. *Europhysics Letters*, 35:61–66, 1996.
- <sup>25</sup> Hamed Koochaki Kellardeh, Vadym Apalkov, and Mark I. Stockman. Wannier-stark states of graphene in strong electric field. *Physical Review B - Condensed Matter and Materials Physics*, 90, 2014.
- <sup>26</sup> Hamed Koochaki Kellardeh, Vadym Apalkov, and Mark I. Stockman. Graphene in ultrafast and superstrong laser fields. *Physical Review B - Condensed Matter and Materials Physics*, 91:1–8, 2015.
- <sup>27</sup> François Fillion-Gourdeau, Denis Gagnon, Catherine Lefebvre, and Steve MacLean. Time-domain quantum interference in graphene. *Physical Review B*, 94(12):125423, September 2016. Publisher: American Physical Society.

- <sup>28</sup> C. Lefebvre, D. Gagnon, F. Fillion-Gourdeau, and S. MacLean. Carrier-envelope phase effects in graphene. *JOSA B*, 35(4):958–966, April 2018.
- <sup>29</sup> Denis Gagnon, Joey Dumont, François Fillion-Gourdeau, and Steve MacLean. Pulse shaping in the terahertz frequency range for the control of photo-excited carriers in graphene. *Journal of the Optical Society of America B*, 35(12):3021, December 2018.
- <sup>30</sup> P. Elliott, T. Müller, J. K. Dewhurst, S. Sharma, and E. K. U. Gross. Ultrafast laser induced local magnetization dynamics in Heusler compounds. *Scientific Reports*, 6:38911, December 2016.
- <sup>31</sup> Erich Runge and E. K. U. Gross. Density-functional theory for time-dependent systems. *Phys. Rev. Lett.*, 52:997–1000, Mar 1984.
- <sup>32</sup> C. A. Ullrich. *Time-Dependent Density-Functional Theory Concepts and Applications*. Oxford University Press, Oxford, New York, 2011.
- <sup>33</sup> M.A.L. Marques, N.T. Maitra, F. Nogueira, E.K.U. Gross, and A. Rubio. *Fundamentals of Time-Dependent Functional Theory*. Springer-Verlag, Berlin, Heidelberg, 2012.
- <sup>34</sup> D. J. Singh. *Planewaves Pseudopotentials and the LAPW Method*. Kluwer Academic Publishers, Boston, 1994.
- <sup>35</sup> J. K. Dewhurst, S. Sharma, and et al., Jan. 14 **2018**.
- <sup>36</sup> K. Krieger, J. K. Dewhurst, P. Elliott, S. Sharma, and E. K. U. Gross. Laser-induced demagnetization at ultra-short time scales: Predictions of tddft. *Journal of Chemical Theory and Computation*, 11(10):4870–4874, 2015.
- <sup>37</sup> J.K. Dewhurst, K. Krieger, S. Sharma, and E.K.U. Gross. An efficient algorithm for time propagation as applied to linearized augmented plane wave method. *Computer Physics Communications*, 209:92 – 95, 2016.
- <sup>38</sup> S. Azar Oliaei Motlagh, Fatemeh Nematollahi, Aranyo Mitra, Ahmal Jawad Zafar, Vadym Apalkov, and Mark I. Stockman. Ultrafast optical currents in gapped graphene. *Journal of Physics: Condensed Matter*, 32(6):065305, November 2019.